

ear Schrödinger equation in the form of bright and dark solitons are obtained for AD and ND respectively when the nonlinearity is strictly positive. Unlike bright and dark Kerr solitons, the DSs are found in all four domains (including negative nonlinearity) followed by the governing equation in the form of a complex Ginzburg-Landau equation (GLE). We observe that, in domain 1 and 3 (where multiplication of GVD coefficient β_2 and nonlinear parameter γ gives positive value) the DSs exhibit flat-top spectra and are robust in nature. On the other hand, in domain 2 and 4 (where multiplications of β_2 and γ gives negative value) the shape of the DS spectra exhibits standard *sech* form. We exploit the variational treatment [12–16] to theoretically investigate the effects of physical perturbations like intra-pulse Raman scattering (IRS), self-steepening, third-order dispersion (TOD) and ZNP on the propagation of stable DS. The variational technique is a standard method used extensively in solving soliton problem in dissipative systems where the perturbations are included suitably into the Lagrangian density [12]. The problem is further reduced by integrating the Lagrangian density followed by the Ritz optimization that leads to the equations of motion of individual pulse parameters under the perturbation. In our variational treatment we include the effect of the ZNP as a perturbation and investigate its effect. We further notice, the ZNP not only restricts or enhances the frequency down-shifting due to IRS, it also modifies the frequency location of TOD-mediated radiations. We theoretically investigate this phenomenon and establish a phase matching (PM) equation that predicts the spectral location of radiation frequency under ZNP.

We organize the work as follows; in Sec. II, we introduce a realistic active waveguide that exhibits strong frequency dependent nonlinearity and can excite DS. In such a waveguide in addition to zero GVD wavelength we have zero-nonlinearity wavelength. We show that for such waveguide, based on the numeric signs of β_2 and γ , one can construct four operational regimes and DS can be excited in all four domains. In Sec. III, we show the analytical results obtained from the variation analysis. In Sec. IV, we study the impact of ZNP on IRS and correlate the numerical data with the variational results. Finally in Sec. V, we study how ZNP modifies the TOD-mediated radiation excited from DS [17]. We establish a modified PM equation that predicts the location of radiation as a function of the ZNP.

II. THE GINZBURG-LANDAU EQUATION WITH NEGATIVE NONLINEARITY

We propose an active Si-based waveguide shown in Fig. 1(a) whose core is doped with silver nanoparticles. For this waveguide, the dispersion and nonlinear profiles are shown in Fig. 1(b) for the wavelength range 1.2 – 2.4 μm . By changing the geometry of the waveguide and density of doped nanoparticles we can tailor the posi-

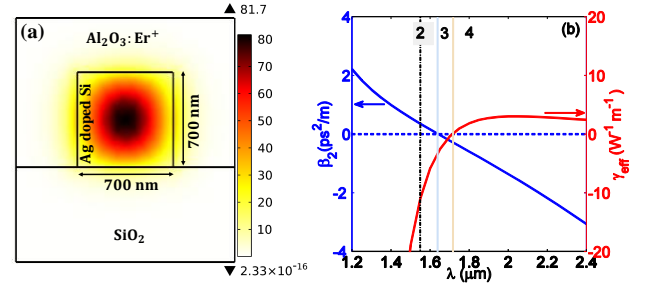


FIG. 1. (a) Cross section of the proposed waveguide and transverse confinement of the quasi-TE mode is shown for $\lambda_0 = 1.55 \mu\text{m}$ (domain 2) for a filling factor of $f = 6 \times 10^{-3}$. The width and height of the waveguide are $h = 700 \text{ nm}$ and $w = 700 \text{ nm}$, respectively. (b) The GVD and the nonlinear profiles are shown by the solid blue line and solid red line respectively. The location of the input wavelength ($\lambda_0 = 1.55 \mu\text{m}$) is shown by the vertical dotted line. The domains 2, 3 and 4 are separated by the zero GVD and zero nonlinearity wavelengths.

tions of zero GVD wavelength and ZNP, which leads to four different operational domains. It is assumed that the doped nanoparticles solely influences the Kerr nonlinearity and the Raman contribution remains unaffected [8, 9]. With this assumption, the GLE for optical field envelope $A(z, t)$ is written as,

$$i \frac{\partial A}{\partial z} + \sum_{n=1}^{\infty} \frac{i^n \beta_n}{n!} \frac{\partial^n A}{\partial t^n} - i \left(G + G_2 \frac{\partial^2}{\partial t^2} \right) A + i \alpha_l A + (1 - f_R) \gamma_{eff}(\omega) |A(z, t)|^2 A(z, t) + f_R \gamma(\omega) \times \left(A(z, t) \int_0^{\infty} h_R(t') |A(z, t - t')|^2 dt' \right) = 0, \quad (1)$$

where β_n is the n^{th} -order dispersion parameter and the nonlinear parameter of the undoped medium is $\gamma(\omega) = \gamma_R(\omega) + i\gamma_I(\omega)$ with $\gamma_R(\omega)$ and $\gamma_I(\omega)$ are the real and imaginary parts respectively. The $\gamma_R(\omega)$ term gives the self-phase modulation effect and the $\gamma_I(\omega)$ gives the nonlinear absorption loss which, in our case, is the two-photon absorption (TPA) loss and assumed to be independent of ω . G and G_2 are the gain and gain dispersion coefficient, α_l is the linear loss coefficient and f_R is the fractional Raman contribution. The term $\gamma_{eff}(\omega)$ is the nonlinear parameter of the doped medium. We can expand $\gamma_R(\omega)$ and $\gamma_{eff}(\omega)$ in the Taylor's series as: $\gamma_R(\omega) \approx \gamma_0 + \gamma_1(\omega - \omega_0)$ and $\gamma_{eff}(\omega) \approx \gamma_{0eff} + \gamma_{1eff}(\omega - \omega_0)$. The parameters are defined as $\gamma_R(\omega) = \frac{2\pi n_2(\omega)}{\lambda_0 A_{eff}}$, $\gamma_I = \frac{\beta_{TPA}}{2A_{eff}}$, $\gamma_{eff}(\omega) = \frac{2\pi n_{2eff}(\omega)}{\lambda_0 A_{eff}}$, $\gamma_1 \approx \frac{\gamma_0}{\omega_0}$, $n_2 = \frac{3\chi_h^{(3)}}{4\epsilon_0 n^2 c}$ and $n_{2eff} = \frac{3\chi_{eff}^{(3)}}{4\epsilon_0 c \epsilon_{eff}}$, where λ_0 is the pump wavelength and β_{TPA} is the TPA coefficient. Here $\epsilon_{eff} = \frac{\epsilon_h(1+2\sigma f)}{(1-\sigma f)}$ with $\sigma = \frac{\epsilon_i - \epsilon_h}{\epsilon_i + 2\epsilon_h}$ is the effective permittivity of the silver-doped medium (in our case it is Si-based active waveguide) calculated from Maxwell-Garnett theory [18]. The

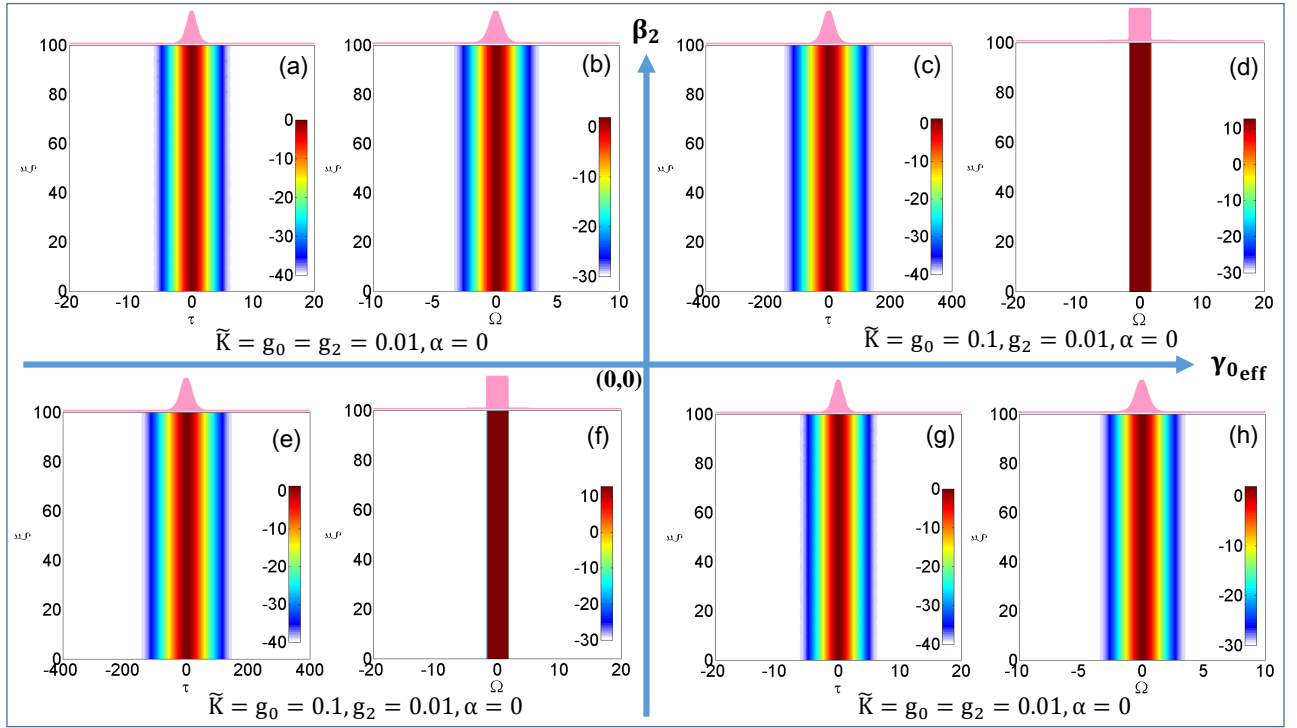


FIG. 2. Temporal and spectral dynamics of the exact solution Eq. (4) of the unperturbed GLE in four different nonlinear dispersive domains. The evolution of DS in (a) Temporal and (b) spectral domain where the GVD is normal ($\beta_2 > 0$) and nonlinearity is self-defocussing type ($\gamma_{0eff} < 0$) (domain 2). The same evolutions are described in (c)-(d); (e)-(f) and (g)-(h), where the GVD and nonlinearities are ($\beta_2 > 0, \gamma_{0eff} > 0$); ($\beta_2 < 0, \gamma_{0eff} < 0$) and ($\beta_2 < 0, \gamma_{0eff} > 0$), and denoted by the domains 1; 3 and 4 respectively. Here $\Omega = 2\pi(\nu - \nu_0)t_0$. The pulse shape on top of each panel gives the corresponding output intensity of stable DS.

filling factor f depends on the density of silver nanoparticles. Further, ε_i and ε_h are the dielectric functions of silver [19] and Si, respectively. The effective third-order susceptibility of silver-doped Si waveguides has been calculated using the theory of composite nonlinear materials [20] as,

$$\chi_{eff}^{(3)} = f \frac{\chi_i^{(3)}}{|B|^2 B^2} + \chi_h^{(3)} \frac{D}{|1 - f\sigma|^2 (1 - f\sigma^2)^2} \quad (2)$$

with $B = \frac{(1-\sigma f)(\varepsilon_i + 2\varepsilon_h)}{3\varepsilon_h}$ and $D = 1 - f \left\{ 1 - 0.4(4\sigma^2|\sigma|^2 + 3\sigma|\sigma|^2 + \sigma^3 + 9|\sigma|^2 + 9\sigma^2) \right\}$.

$\chi_h^{(3)}$ is the susceptibility of host Si. The susceptibility of silver is $\chi_i^{(3)} = (-6.3 + i1.9) \times 10^{-16} m^2/V^2$. The cross-section of the fundamental field distribution is shown in Fig. 1(a). We use COMSOL software for a filling factor of $f = 6 \times 10^{-3}$ to obtain the GVD and nonlinear profiles. To study the impact of individual perturbations on a DS we reduce the integral form of GLE (Eq. (1)) to a more convenient discrete form. The discrete form of the extended GLE (upto 1st order in

γ_{eff}) is normalized as,

$$\begin{aligned} i \frac{\partial u}{\partial \xi} - \frac{1}{2} \text{sgn}(\beta_2) \frac{\partial^2 u}{\partial \tau^2} - i \left(g_0 + g_2 \frac{\partial^2}{\partial \tau^2} \right) u + i \alpha u \\ + \{ \text{sgn}(\gamma_{0eff}) + i K f_R \} |u|^2 u = i \delta_3 \frac{\partial^3 u}{\partial \tau^3} + \tau_R \Gamma_0 u \frac{\partial |u|^2}{\partial \tau} \\ + \{ \text{sgn}(\gamma_{0eff}) - \Gamma_0 \} f_R |u|^2 u - i \{ \mu_{1eff} (1 - f_R) \\ + \Gamma_0 s f_R \} \frac{\partial (|u|^2 u)}{\partial \tau}, \quad (3) \end{aligned}$$

where $\Gamma_0 = \gamma_0/\gamma_{0eff}$, $\mu_{1eff} = \gamma_{1eff}/(|\gamma_{0eff}|t_0)$. The time and space variables are normalized as $\tau = (t - z v_g^{-1})/t_0$ and $\xi = z/L_D$, where v_g is the group velocity of the pulse, t_0 is the initial pulse width and $L_D = t_0^2/|\beta_2(\omega_0)|$ is the dispersion length, $\beta_2(\omega_0)$ being the GVD coefficient at the carrier frequency ω_0 . The TOD, IRS and self-stepping parameters are normalized as $\delta_3 = \beta_3/(3!|\beta_2|t_0)$, $\tau_R = T_R/t_0$ and $s = 1/(\omega_0 t_0)$, where T_R is the first moment of the Raman response function [2]. The field amplitude A is rescaled as, $A = u\sqrt{P_0}$, where peak power $P_0 = |\beta_2(\omega_0)|/(t_0^2 \gamma_R)$. The dimensionless TPA coefficient is given as, $K = \gamma_I/\gamma_R = \beta_{TPA} \lambda_0/(4\pi n_2)$. The α_l , G and G_2 are normalized as $\alpha = \alpha_l L_D$, $g_0 = G L_D$ and $g_2 = g_0 (T_2/t_0)^2$ respectively, where dephasing time is T_2 . Note that, if we omit the right-side of Eq. (3) then it will readily reduce to the well-known unperturbed GLE

for which we have an exact solution of the form of PS soliton [11]

$$u(\xi, \tau) = u_0 [\operatorname{sech}(\eta\tau)]^{(1+ia)} e^{i\Gamma\xi}, \quad (4)$$

where the four parameters u_0 , η , a and Γ satisfy the following relations:

$$\begin{aligned} |u_0|^2 &= \frac{g_0 - \alpha}{\tilde{K}} \left[1 - \frac{\operatorname{sgn}(\beta_2)a/2 + g_2}{g_2(a^2 - 1) - \operatorname{sgn}(\beta_2)a} \right], \\ \eta^2 &= \frac{g_0 - \alpha}{g_2(a^2 - 1) - \operatorname{sgn}(\beta_2)a}, \\ \Gamma &= \frac{\eta^2}{2} [\operatorname{sgn}(\beta_2)(a^2 - 1) + 4ag_2], \\ a &= \frac{H - \operatorname{sgn}(\gamma_{0eff})\sqrt{H^2 + 2\delta^2}}{\delta}, \end{aligned} \quad (5)$$

with $H = -[(3/2)\operatorname{sgn}(\beta_2) + 3g_2\tilde{K}\operatorname{sgn}(\gamma_{0eff})]$, $\delta = -[2g_2 - \operatorname{sgn}(\beta_2)\operatorname{sgn}(\gamma_{0eff})\tilde{K}]$ and $\tilde{K} = K$, when the medium is undoped (nonlinearity is self-focusing type) and $\tilde{K} = Kf_R$, when the medium is doped with silver nanoparticles (nonlinearity is self-defocusing or self-focusing type depending on the location of the ZNP). The numerical solution of unperturbed GLE (all the RHS terms = 0 for Eq. (3)) is shown in Fig. 2. Depending on the numeric signs of β_2 and γ_{0eff} we can define four different regimes to excite DS. The numerical solution shows that the DSs are robust in all four domains and propagate without any distortion. In each case we launch pure PS soliton as input whose parameters obey the relationship shown in Eq. (5). The full numerical solution reveals that, the same sign of the products of $\operatorname{sgn}(\beta_2)$ and $\operatorname{sgn}(\gamma_{0eff})$ give rise to identical structure of DS. In Fig. 2, the set (a)-(b) has the identical structures as (g)-(h) (here, $\operatorname{sgn}(\beta_2 \times \gamma_{0eff}) = -1$ for both the cases). Similarly the set (c)-(d) and (e)-(f) are identical. For the second case, in Fig. 2 (d) and (f), a flat-top spectrum is observed in frequency domain of DS when both the GVD and nonlinearity have the same sign or their product is positive ($\operatorname{sgn}(\beta_2 \times \gamma_{0eff}) = +1$). Interestingly, the temporal width of such DS is found to be much wider compare to the previous case.

III. VARIATIONAL ANALYSIS

The stable PS soliton evolves when the right-hand side of Eq. (3) vanishes. But it is interesting to study how the perturbations affect the stable PS soliton propagating under self-focusing and self-defocusing nonlinearity. To grasp the role of higher-order effects and negative nonlinearity, we study their impact through a variational analysis by treating them as small perturbations. The variation method is a standard technique which relies on the assumption that the overall shape of the input pulse remain unaffected during propagation. However, different pulse parameters like width, amplitude, phase,

frequency, chirp etc. can vary. The choice of ansatz is an important step in such treatment [2]. In order to get the equation of motion of different pulse parameters, we first write Eq. (3) in the form of a perturbed nonlinear Schrödinger equation:[2, 15]

$$i\frac{\partial u}{\partial \xi} - \frac{1}{2}p\frac{\partial^2 u}{\partial \tau^2} + q|u|^2u = i\epsilon(u), \quad (6)$$

where $p = \operatorname{sgn}(\beta_2)$, $q = \operatorname{sgn}(\gamma_{0eff})$ and the small perturbation $\epsilon(u)$ is defined as,

$$\begin{aligned} \epsilon(u) &= \delta_3 \frac{\partial^3 u}{\partial \tau^3} - i\tau_R \Gamma_0 u \frac{\partial |u|^2}{\partial \tau} - \{\mu_{1eff}(1 - f_R) \\ &+ \Gamma_0 s f_R\} \frac{\partial (|u|^2 u)}{\partial \tau} - i(q - \Gamma_0) f_R |u|^2 u \\ &- K f_R |u|^2 u + g_0 u + g_2 \frac{\partial^2 u}{\partial \tau^2}. \end{aligned} \quad (7)$$

For this specific problem, we choose the PS soliton (see Eq. (4)) as our ansatz since it is the exact solution of Eq. (3) in absence of all the perturbations. The complete mathematical form of the ansatz is as follows,

$$u(\xi, \tau) = u_0(\xi) (\operatorname{sech}[\eta(\xi) \{\tau - \tau_p(\xi)\}]^{1+ia(\xi)}) \exp(i[\phi(\xi) - \Omega_p(\xi) \{\tau - \tau_p(\xi)\}]). \quad (8)$$

Note, the six parameters u_0 , η , τ_p , ϕ , a and Ω_p are now assumed to be a function of ξ . Next we introduce a Lagrangian density appropriate for Eq. (6) as, $\mathcal{L}_D = \frac{i}{2}(uu_\xi^* - u^*u_\xi) - \frac{1}{2}(q|u|^4 + p|u_\tau|^2)$. We integrate \mathcal{L}_D over τ using the ansatz given in Eq. (8) and obtain the following reduced Lagrangian:

$$\begin{aligned} L &= \int_{-\infty}^{\infty} \mathcal{L}_D d\tau = \frac{2u_0^2}{\eta} \left(\frac{\partial \phi}{\partial \xi} + \Omega_p \frac{\partial \tau_p}{\partial \xi} \right) - \frac{au_0^2}{\eta^2} \frac{\partial \eta}{\partial \xi} \\ &+ C \frac{u_0^2}{\eta} \frac{\partial a}{\partial \xi} - p \frac{\eta u_0^2}{3} (1 + a^2) - \frac{u_0^2}{\eta} \left(p \Omega_p^2 + q \frac{2}{3} u_0^2 \right) \\ &+ i \int_{-\infty}^{\infty} (\epsilon u^* - \epsilon^* u) d\tau, \end{aligned} \quad (9)$$

where $C = [\ln(4) - 2]$. Finally we use the Euler-Lagrange equation for each pulse parameter to obtain a set of coupled ODEs for the six parameters that describe the overall soliton dynamics [2, 21]. These equations describe the evolution of pulse energy ($E = \int_{-\infty}^{\infty} |u|^2 d\tau$), temporal position τ_p , frequency shift Ω_p , amplitude η , frequency chirp a , and phase ϕ with the following form,

$$\frac{dE}{d\xi} = \frac{d}{d\xi} \left(\frac{2u_0^2}{\eta} \right) = 2\operatorname{Re} \int_{-\infty}^{\infty} \epsilon u^* d\tau, \quad (10)$$

$$\frac{d\tau_p}{d\xi} = p \Omega_p + \frac{\eta}{u_0^2} \int_{-\infty}^{\infty} (\tau - \tau_p) \operatorname{Re}(\epsilon u^*) d\tau, \quad (11)$$

$$\frac{d\Omega_p}{d\xi} = \frac{\eta^2}{u_0^2} \int_{-\infty}^{\infty} \tanh[\eta(\tau - \tau_p)] \operatorname{Re}[(a + i)\epsilon u^*] d\tau, \quad (12)$$

$$\frac{d\eta}{d\xi} = -C \frac{\eta^2}{2u_0^2} E_\xi - p \frac{2\eta^3 a}{3} + \frac{2\eta^2}{u_0^2} \times \int_{-\infty}^{\infty} \ln[\operatorname{sech}\{\eta(\tau - \tau_p)\}] \operatorname{Re}(\epsilon u^*) d\tau, \quad (13)$$

$$\frac{da}{d\xi} = -\frac{2\eta^2}{u_0^2} \operatorname{Im} \int_{-\infty}^{\infty} (\tau - \tau_p) \tanh[\eta(\tau - \tau_p)] (1 - ia) \epsilon u^* d\tau - \frac{a\eta}{2u_0^2} E_\xi + q \frac{2}{3} u_0^2 + p \frac{2}{3} \eta^2 (1 + a^2) + \frac{\eta}{u_0^2} \operatorname{Im} \int_{-\infty}^{\infty} \epsilon u^* d\tau, \quad (14)$$

$$\frac{d\phi}{d\xi} = \frac{a}{2\eta} \eta_\xi - \frac{C}{2} a_\xi - \Omega_p \tau_{p\xi} + \frac{2}{3} q u_0^2 + \frac{1}{6} p \eta^2 (1 + a^2) + \frac{1}{2} p \Omega_p^2 + \frac{\eta}{2u_0^2} \operatorname{Im} \int_{-\infty}^{\infty} \epsilon u^* d\tau, \quad (15)$$

where Re and Im stand for real and imaginary parts. The final step is to evaluate all the integrals using $\epsilon(u)$ given in Eq. (7). It results in the following set of six coupled differential equations:

$$\frac{dE}{d\xi} = \frac{2}{3} (3g_0 - K f_R \eta E) E - \frac{2}{3} g_2 [(1 + a^2) \eta^2 + 3\Omega_p^2] E, \quad (16)$$

$$\frac{d\tau_p}{d\xi} = (p - 2g_2 a) \Omega_p + \frac{1}{2} \{ \mu_{1eff} (1 - f_R) + \Gamma_0 s f_R \} \eta E + \delta_3 [(1 + a^2) \eta^2 + 3\Omega_p^2], \quad (17)$$

$$\frac{d\Omega_p}{d\xi} = -\frac{4}{3} g_2 (1 + a^2) \Omega_p \eta^2 - \frac{4}{15} \tau_R \Gamma_0 E \eta^3 + \frac{4}{15} \{ \mu_{1eff} (1 - f_R) + \Gamma_0 s f_R \} a E \eta^3, \quad (18)$$

$$\frac{d\eta}{d\xi} = -\frac{2}{9} (3p a \eta + E K f_R) \eta^2 - \frac{4}{9} (2 - a^2) g_2 \eta^3 - 4\delta_3 a \Omega_p \eta^3, \quad (19)$$

$$\frac{da}{d\xi} = \frac{1}{3} \{ q(1 - f_R) + (K a + \Gamma_0) f_R \} E \eta + \frac{2}{3} (p - g_2 a) (1 + a^2) \eta^2 + 4\delta_3 \Omega_p \eta^2 (1 + a^2) + \frac{1}{3} \{ \mu_{1eff} (1 - f_R) + \Gamma_0 s f_R \} \Omega_p \eta E, \quad (20)$$

$$\frac{d\phi}{d\xi} = \frac{a}{2\eta} \eta_\xi - \frac{C}{2} a_\xi - \Omega_p \tau_{p\xi} + \frac{1}{3} q \eta E + \frac{1}{6} p \eta^2 (1 + a^2) + \frac{1}{2} p \Omega_p^2 + \frac{1}{3} \{ \mu_{1eff} (1 - f_R) + \Gamma_0 s f_R \} \Omega_p E \eta - \frac{1}{3} (q - \Gamma_0) f_R E \eta + \delta_3 [(1 + a^2) \Omega_p \eta^2 + \Omega_p^3]. \quad (21)$$

These equations are quite significant to understand the pulse dynamics. Each equation provides considerable physical insight as they show how a perturbation affects a specific pulse parameter. For example, the Raman parameter τ_R appears only in the equation for the frequency

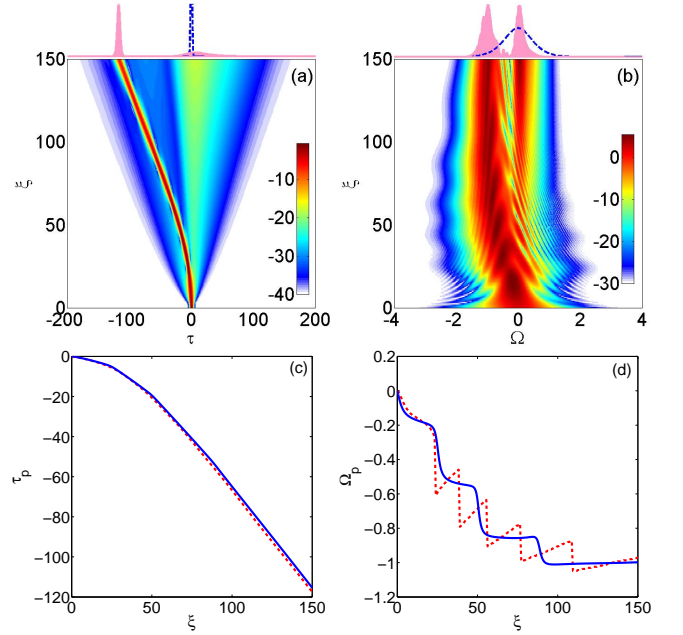


FIG. 3. (Color online) (a) Temporal and (b) spectral evolution of the perturbed DS in domain 2 ($\beta_2 > 0$ and $\gamma_{0eff} < 0$) for the parameters $K = 0.05$, $g_0 = g_2 = 0.01$, $\Gamma_0 = 0.2$, $f_R = 0.245$, $\tau_R = 0.5$, $s = 0.1$ and $\mu_{1eff} = -0.1$. The input (dotted trace) and output pulse shapes are also shown in the top panel. Variation of (c) temporal peak position shift (τ_p) and (d) frequency position shift (Ω_p) over the propagation distance. The solid lines give the variational results, whereas the dotted lines give the numerically simulated results.

shift Ω_p and the term containing it has a negative sign. This immediately shows that the IRS leads to a spectral redshift of the DS. The term μ_{1eff} appears in the frequency equation which modifies the self-steepening parameter s and depending on the signs of μ_{1eff} the Raman redshift will be restricted (for $\mu_{1eff} < 0$) or relaxed more (for $\mu_{1eff} > 0$). The presence of the term μ_{1eff} in the equations of temporal position τ_p and frequency chirp a will also modify the dynamics of DS.

IV. INFLUENCE OF THE ZNP ON RAMAN REDSHIFT

The impact of ZNP is significant on Raman redshift. Suppression of Raman red-shifting due to two-zero dispersion is a well-known phenomenon in Kerr solitons where strong dispersive waves are generated across the second zero GVD point [22]. Recently, it is observed that the Raman red-shifting of Schrödinger Kerr soliton is also restricted in the presence of ZNP [8, 9]. However, this suppressed Raman frequency shift does not lead to any other radiation across ZNP. In other words, in this case the ZNP acts as a perfect barrier that not only restricts the Raman redshift but also does not allow any radiation beyond this point. The earlier reported works [8, 9] on ZNP are mostly based on numerical observations with less theoretical explanation. Here we try to

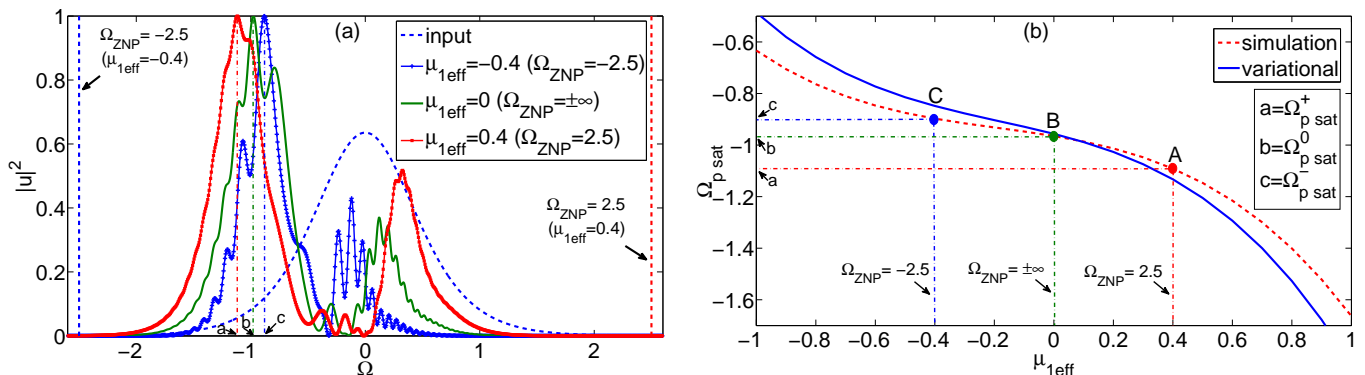


FIG. 4. (Color online) (a) Raman induced spectral redshift for $\mu_{1eff} = 0, \pm 0.4$ at $\xi = 100$. (b) $\Omega_{p sat}$ as a function of μ_{1eff} plot. The parameters used in the simulations are the same as Fig. 3.

address this specific problem theoretically for DSs which experiences the ZNP. Like Kerr solitons, the impact of IRS term is characteristically same for DSs where we get frequency red-shifting. To study the impact of IRS, we exclude the TOD term (i.e., $\delta_3 = 0$) and numerically solve the extended GLE Eq. (3) using the standard split-step Fourier method [2]. The input pulse is taken in the form of a PS soliton whose parameters obey the relations shown in Eq. (5). Finally the full numerical results are compared with the results obtained from the variational method by solving the set of coupled ordinary differential equations Eqs. (16)-(20). Figures. 3(a) and (b) show the density plots of temporal and spectral evolution of an optical DS under IRS. The temporal position (τ_p) and frequency shift (Ω_p) with respect to the propagation distance are also plotted in Figs. 3(c) and (d) respectively, where results from variational analysis and full numerical simulation are superimposed. The variational results (solid lines) corroborate well with the full numerical results (dotted lines). Next, we try to understand the influence of ZNP on Raman redshift. The slope of the nonlinear dispersion curve is mathematically defined by the parameter μ_{1eff} . Note that, the value of the slope (μ_{1eff}) determines the location of the ZNP. In Fig. 4, we plot the output spectrum for three different cases where the values of $\mu_{1eff} = 0, \pm 0.4$. When $\mu_{1eff} = 0$, the nonlinear dispersion curve is independent of frequency and does not contain any ZNP. In such case, the DS accelerates freely and its spectrum is shown by the solid green line in Fig. 4(a). Now, the Raman redshift is reduced significantly when a ZNP is introduced with a negative slope ($\mu_{1eff} = -0.4$). The location of the ZNP is shown by a vertical blue dotted line and it behaves like a barrier that restricts the frequency down-shifting. Interestingly, the redshift is enhanced (red line) when a ZNP is located beyond the launching point in positive frequency side (denoted by a vertical red dotted line). In order to understand this phenomena quantitatively, we exploit the variational results. It is observed that, the frequency red-shifting due to IRS is saturated over the distance. This saturated frequency is denoted by $\Omega_{p sat}$. The full variational treatment can predict $\Omega_{p sat}$, which is a function

of μ_{1eff} . In Fig. 4(a), the peak frequency positions are denoted by $a = \Omega_{p sat}^+$ (for $\mu_{1eff} = +0.4$), $b = \Omega_{p sat}^0$ (for $\mu_{1eff} = 0$) and $c = \Omega_{p sat}^-$ (for $\mu_{1eff} = -0.4$). In Fig. 4(b) we try to map the results obtained in Fig. 4(a), where we use the simulated values to plot $\Omega_{p sat}$ as a function of μ_{1eff} . In Fig. 4(b), we also locate the three points A, B and C for $\mu_{1eff} = +0.4, 0$ and -0.4 , respectively. We superimpose the variational result (solid blue line) in the same plot, and find a close agreement between them. The physical origin of suppressed and enhanced Raman redshift can be explained from asymmetric pulse broadening due to frequency dependent nonlinearity [2]. The term μ_{1eff} acts as a modulation to the self-steepening strength and even changes its sign. When $\mu_{1eff} > 0$ (< 0), it increases (decreases) the total self-steepening strength and under self-defocussing nonlinearity, it gives a small frequency shift towards lower (higher) frequency side, and this effect results in enhanced (suppressed) Raman redshift combining with IRS perturbation. This is also validated from variational method by the Eq. (18).

V. DISSIPATIVE SOLITON MEDIATED RADIATION UNDER THE ZNP

The TOD is the primary perturbation that a soliton experiences when it propagates through a dispersive medium. Being an asymmetric term, TOD leads to some temporal side-lobes and is responsible for generating a phase-matched radiation in the form of a DW [23]. In one of our previous works, it has already been shown that like Kerr soliton, the DS can also radiate DW in the vicinity of zero GVD wavelength [17]. However, the situation is rather interesting when DS experiences a ZNP in addition to the zero GVD wavelength. The relative location of the zero GVD wavelength and ZNP compared to the input wavelength significantly influences the dynamics of the DS. We solve the GLE numerically considering TOD as perturbation, and the simulated results are shown in Fig. 5. The formation of DW across the zero GVD point (shown by a vertical dotted line) is evident. We run our simulation in presence and in absence of ZNP

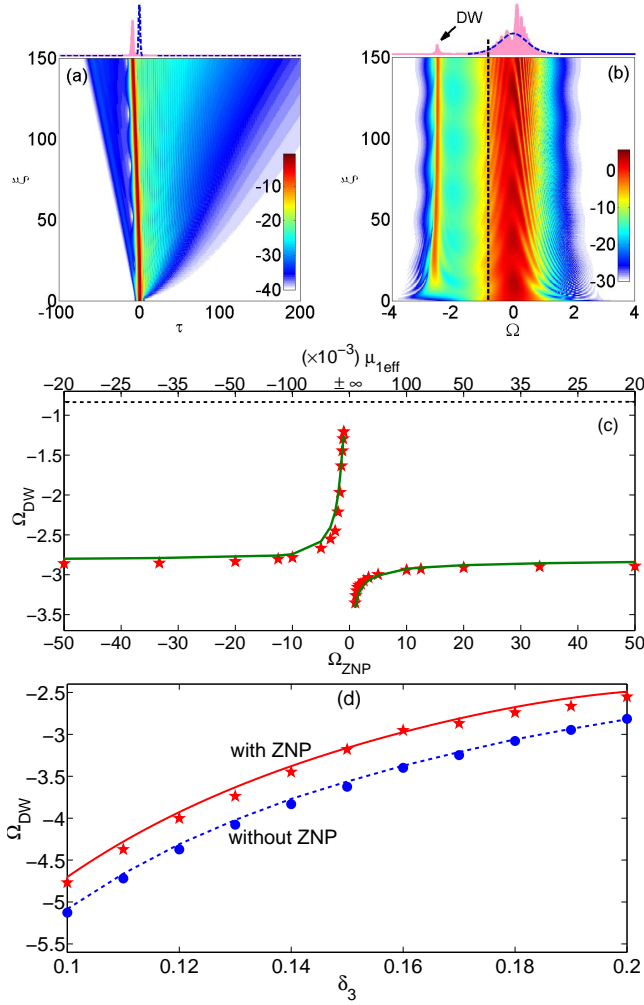


FIG. 5. (Color online) (a) Temporal and (b) spectral evolution of DS in presence of TOD ($\delta_3 = 0.2$) and ZNP ($\mu_{1eff} = -0.1$) along with all other perturbation values same as Fig. 3. The input (dotted trace) and output pulse shapes are also shown in the top panel. (c) The variation of the frequency location of DW (Ω_{DW}) with the variation of ZNP (μ_{1eff}). The solid lines represent the results obtained from the PM equation Eq. (22), whereas the stars give the numerically simulated results. The vertical and horizontal dotted lines in (b) and (c) represent the locations of zero GVD position respectively. (d) The variation of Ω_{DW} with TOD parameter in the presence of ZNP ($\mu_{1eff} = -0.3$) and in the absence ZNP ($\mu_{1eff} = 0$). The stars (circles) give the simulated results, whereas the solid red line (dashed blue line) gives the prediction from the PM equation, when the ZNP is present (absent).

where we find the frequency location of DW is modified by the ZNP. We introduce the effect of ZNP in the PM equation and derive the following equation in normalised unit [17],

$$\frac{sgn(\beta_2)}{2}\Omega^2 + \delta_3\Omega^3 - \tau_g\Omega = 2\Gamma + sgn(\gamma_{0eff})\Gamma\mu_{1eff}\Omega. \quad (22)$$

Here, $\tau_g = (v_{DW}^{-1} - v_{DS}^{-1})t_0|\beta_2|^{-1}$, is the normalized form of the inverse-velocity mismatch between the DS

and DW. The DS ansatz parameter Γ takes the form: $\Gamma \approx \frac{1}{2}sgn(\gamma_{0eff})u_0^2$. The solution (Ω_{DW}) of Eq. (22) provides the radiation frequency of the DW. It is interesting to note that, unlike zero GVD point, ZNP does not lead to any phase-matched radiation. It can be verified from Eq. (22) that, it does not produce any real solution for the given range of μ_{1eff} when $\delta_3 = 0$. In Figs. 5 (a) and (b), we demonstrate the temporal and spectral evolution of DS in presence of the TOD ($\delta_3 = 0.2$) for $\gamma_{0eff} < 0$. To get the complete picture, we include all the perturbations (Raman, self-steeping, etc.) in the simulation. It is observed that the spectral position of the radiation is affected by the location of the ZNP. When the slope of the nonlinear parameter γ is small, the location of the radiation frequency Ω_{DW} hardly depends on the ZNP. However, there is a radical change in the radiation frequency when the ZNP is kept close to the radiation frequency. Numerically we observe that the ZNP acts as a strong barrier when Raman term is present in the GLE, and the radiation frequency can never cross the ZNP. However, in absence of Raman term (i.e. when only TOD term is present) the radiation can cross the ZNP. If we gradually change the value of μ_{1eff} such that the ZNP (Ω_{ZNP}) shifts towards the radiation frequency, then the radiation frequency is also shifted towards the input frequency. It seems like the ZNP drags the radiation towards the input frequency. A sudden change of radiation frequency is observed when the ZNP crosses the input frequency. That means now the ZNP and zero GVD point are in opposite side of the input frequency. Note that, for such condition the DS is excited in same regime ($\beta_2 > 0$ and $\gamma_{0eff} < 0$), but slope of the nonlinear dispersion profile is changed. The change of radiation frequency Ω_{DW} with respect to ZNP is shown in Fig. 5(c). The solid line corresponds to the results that we obtain from our derived PM condition, whereas the stars represent the numerical data. Further we perform a simulation where we gradually shift the zero GVD point towards negative frequency keeping the ZNP fixed. We note that the ZNP reduces the radiation frequency compared to its actual location. Here the *actual* location means the frequency location of the radiation in the absence of ZNP. In order to visualize this effect we plot Ω_{DW} as a function of δ_3 in Fig. 5(d) in presence (red stars) and in absence (blue dots) of ZNP. It is evident that the radiation frequency is reduced in the presence of ZNP, which is in good agreement with the PM equation derived by us (solid red line).

VI. CONCLUSIONS

In this brief report, we demonstrate that the formation of DS is versatile and it can be excited in self-focusing and self-defocusing nonlinear systems with ND and AD. It is noted that the excited DSs exhibit identical nature in the domain where the numeric sign of the multiplication of nonlinear coefficient (γ_{0eff}) and GVD coefficient (β_2) is same. We numerically find when DSs are excited in

the regime $\gamma_{0eff}\beta_2 > 0$, the pulse is quite robust with an unusual flat-top spectra. We further investigate the influence of the higher-order perturbations on the dynamics of DS in the presence of ZNP. We adopt variational treatment to understand the dynamics of the individual pulse parameter during propagation. An extensive calculation leads to a set of coupled differential equation, which are essentially the equation of motion of the pulse parameters. The influence of ZNP is found to be significant, as it behaves like a barrier that does not allow any radiation to pass through it in the presence of IRS. The Raman redshift is arrested by the ZNP and saturates to a given frequency $\Omega_{p,sat}$. This happens when the ZNP and Raman red-shifted frequency are in the same side of the input frequency. The situation is reversed when the Raman red-shifted frequency and the ZNP are in the opposite sides of the input frequency. In such a situation the ZNP pushes the Raman frequency more towards lower frequency side, and we obtain enhanced red-shifting. The variational treatment theoretically predicts the $\Omega_{p,sat}$ that matches well with the numerical data. A

similar phenomenon is observed for TOD mediated radiation under ZNP. The location of the radiation frequency is influenced by the ZNP. We establish an analytic expression that predicts the radiation frequency in the presence of ZNP. It is considered that the phase-matched radiation is sandwiched between ZNP and zero GVD point. When the ZNP is moved towards zero GVD point, it (ZNP) drags the radiation towards zero GVD point. The concept of negative nonlinearity is relatively new for DS, and it produces some interesting effects like formation of DS in ND, and modulation of Raman redshift and phase-matched radiation through ZNP. In our work, we aim to explore the behaviour of DS under self-defocusing nonlinearity and the role of ZNP. The existence of the negative nonlinearity adds new degrees of freedom in manipulating the pulse dynamics in waveguides and can be useful in practical applications.

ACKNOWLEDGMENTS

A.S. acknowledges MHRD, India for a research fellowship.

-
- [1] N. Akhmediev and A. Ankiewicz, *Dissipative Soliton: Lecture Notes in Physics*, (Springer, Berlin, 2005).
- [2] G. P. Agrawal, *Nonlinear Fiber Optics*, 5th ed. (Academic Press, 2013).
- [3] A.D. Boardman and A. P. Sukhorukov, *Soliton-driven Photonics, (Chapter 'General theory of Solitons' by N. Akhmediev)* (Springer-Science, 2001).
- [4] J. Xu, S. Wu, H. Li, J. Liu, R. Sun, F. Tan, Q. Yang, and P. Wang, "Dissipative soliton generation from a graphene oxide mode-locked Er-doped fiber laser," *Opt. Express* **20**, 23653-23658 (2012).
- [5] B. G. Bale, J. N. Kutz, A. Chong, W. H. Renninger, and F. W. Wise, "Spectral filtering for high-energy mode-locking in normal dispersion fiber lasers," *J. Opt. Soc. Am. B* **25**, 17631770 (2008).
- [6] W. H. Renninger, A. Chong, and F. W. Wise, "Dissipative solitons in normal-dispersion fiber laser," *Phys. Rev. A* **77**, 023814 (2008).
- [7] S. Bose, R. Chattopadhyay, S. Roy, and S. K. Bhadra, "Study of nonlinear dynamics in silver nanoparticle-doped photonic crystal fiber, *JOSA B* **33**, 1014 (2016).
- [8] S. Bose, A. Sahoo, R. Chattopadhyay, S. Roy, S. K. Bhadra, and G. P. Agrawal, "Implications of a zero-nonlinearity wavelength in photonic crystal fibers doped with silver nanoparticles," *Phys. Rev. A* **94**, 043835 (2016).
- [9] F. R. Arteaga-Sierra, A. Antikainen, and G. P. Agrawal, "Soliton dynamics in photonic-crystal fibers with frequency-dependent Kerr nonlinearity," *Phys. Rev. A* **98**, 013830 (2018).
- [10] J. Moses and F. W. Wise, "Controllable self-steepening of ultrashort pulses in quadratic nonlinear media," *Phys. Rev. Lett.* **97**, 073903 (2006).
- [11] N. R. Pereira and L. Stenflo, "Nonlinear Schrödinger equation including growth and damping," *Phys. Fluids* **20**, 1733 (1977).
- [12] A. Sahoo, S. Roy, and G. P. Agrawal, "Perturbed dissipative solitons: A variational approach," *Phys. Rev. A* **96**, 013838 (2017).
- [13] A. Bondeson, M. Lisak, and D. Anderson, "Soliton Perturbations: A variational principle for the soliton parameters," *Phys. Scripta* **97**, pp. 479-485 (1979).
- [14] D. J. Kaup and B. M. Malomed, "The variational principle for nonlinear waves in dissipative systems," *Physica D* **87**, pp. 155-159(1995).
- [15] D. Anderson, "Variational approach to nonlinear pulse propagation in optical fibers," *Phys. Rev. A* **27**, 3135 (1983).
- [16] S. C. Cerda, S. B. Cavalcanti, and J. M. Hickmann, "A variational approach of nonlinear dissipative pulse propagation," *Eur. Phys. J. D* **1**, pp. 313-316 (1998).
- [17] A. Sahoo and S. Roy, "Dissipative soliton mediated radiations in active silicon-based waveguides," *J. Opt. Soc. Am. B* **35**, 257-265 (2018).
- [18] J. C. M. Garnett, "Colours in Metal Glasses and in Metallic Films", *Philos. Trans. R. Soc. London* **203**, 385 (1904).
- [19] P. B. Johnson and R. W. Christy, "Optical Constants of the Noble Metals", *Phys. Rev. B* **6**, 4370 (1972).
- [20] J. E. Sipe and R. W. Boyd, "Nonlinear susceptibility of composite optical materials in the Maxwell Garnett model", *Phys. Rev. A* **46**, 1614 (1992).
- [21] H. Hasegawa and Y. Kodama, *Soliton in Optical Communication* (Oxford University Press, 1995).
- [22] D. V. Skryabin, F. Luan, J. C. Knight, and P. St. J. Russell, "Soliton self-frequency shift cancellation in photonic crystal fibers," *Science* **301**, 1705 (2003).
- [23] N. Akhmediev and M. Karlsson, "Cherenkov radiation emitted by solitons in optical fibers," *Phys. Rev. A* **51**, 2602-2607 (1995).